GEOLOGICA BELGICA (2013) 16/1-2: 76-83

Rare earth element and yttrium characteristics of carbonates within the sediment-hosted Luiswishi and Kamoto Cu-Co deposits, Katanga Copperbelt (Democratic Republic of Congo – DRC).

David DEBRUYNE[1], Lieve BALCAEN[2] , Frank VANHAECKE[2] & Philippe MUCHEZ[1]

[1]*Geodynamics and Geofluids Research Group, Department of Earth and Environmental Sciences, K.U. Leuven, Celestijnenlaan 200E, B-3001 Leuven, Belgium*
[2]*Atomic and Mass Spectrometry Research Group, Department of Analytical Chemistry, Ghent University, Krijgslaan 281-S12, B-9000 Ghent, Belgium*

ABSTRACT. The Neoproterozoic Central African Copperbelt is a world-class metallogenic province characterized by sediment-hosted stratiform Cu-Co ore deposits and polymetallic vein-type deposits. Two main mineralization phases have been recognized in the Katanga Copperbelt (Democratic Republic of Congo). The first phase occurred during early to intermediate diagenesis and the second during deep burial and the Lufilian orogeny. The Rare Earth Element and Yttrium (REY) concentrations of gangue dolomites associated with the second mineralization phase at the Kamoto and Luiswishi ore deposits were determined and compared to those of their respective host rocks. Kamoto samples exhibit convex Upper Continental Crust-normalized patterns with a pronounced light REE depletion without significant Eu anomalies and with positive La anomalies. The Luiswishi samples exhibit either progressively increasing REY patterns or ramp-shaped patterns with minor mid REE-heavy REE fractionation, accompanied by pronounced negative Ce and Eu anomalies. These differences suggest that a more intense metamorphic overprint at Luiswishi contributed to the differences with the Kamoto deposit.

KEYWORDS: dolomite, hydrothermal, fluid-rock interaction, remobilization, Eu anomaly, Ce anomaly

1. Introduction

The Neoproterozoic Central African Copperbelt located at the border between Zambia and the Democratic Republic of Congo (DRC) is the world's richest sediment-hosted stratiform Cu-Co province, containing numerous deposits hosting a total of about 200 Mt of copper (Cailteux et al. 2005b) and over 8 Mt of cobalt (Misra, 2000). Conflicting genetic models have been proposed including epigenetic-magmatic (e.g. Bateman, 1930; Davidson, 1931) over synsedimentary (e.g Mendelsohn, 1961; Fleischer et al., 1976), diagenetic (e.g. Bartholomé et al., 1972; Annels, 1989) and epigenetic-synorogenic (e.g. Molak, 1995; McGowan et al., 2003, 2006). Recent papers favor a multistage hypogene mineralization model, involving an early to intermediate diagenetic mineralization followed by a multiphase synorogenic mineralization (e.g. Selley et al., 2005; Cailteux et al., 2005b; Dewaele et al., 2006; El Desouky et al., 2009; Muchez et al., 2010).

This research paper seeks to better understand the nature and evolution of the fluids responsible for Cu-Co mineralization and to better understand fluid-rock reactions during initial mineralization and subsequent remobilization. The focus lies on the REY patterns in the second Cu-Co mineralization at Kamoto and Luiswishi (Fig. 1), two well-studied deposits in the Katanga Copperbelt (e.g. Dewaele et al., 2006; El Desouky et al., 2009, 2010).

2. Geological setting

2.1 Geotectonic context

The Cu-Co deposits of the Copperbelt are hosted by the Katanga Supergroup, a Neoproterozoic sedimentary sequence deposited between >880 and <570 Ma (Armstrong et al., 2005; Master et al., 2005). The Katanga basin that hosts this supergroup is generally considered to be part of an aulacogen, a failed intracontinental rift (e.g. Clemmey, 1974; Porada & Berhorst, 2000). The Roan Group forms the base of the Katanga Supergroup and consists of siliciclastic and carbonate sequences which record the transition

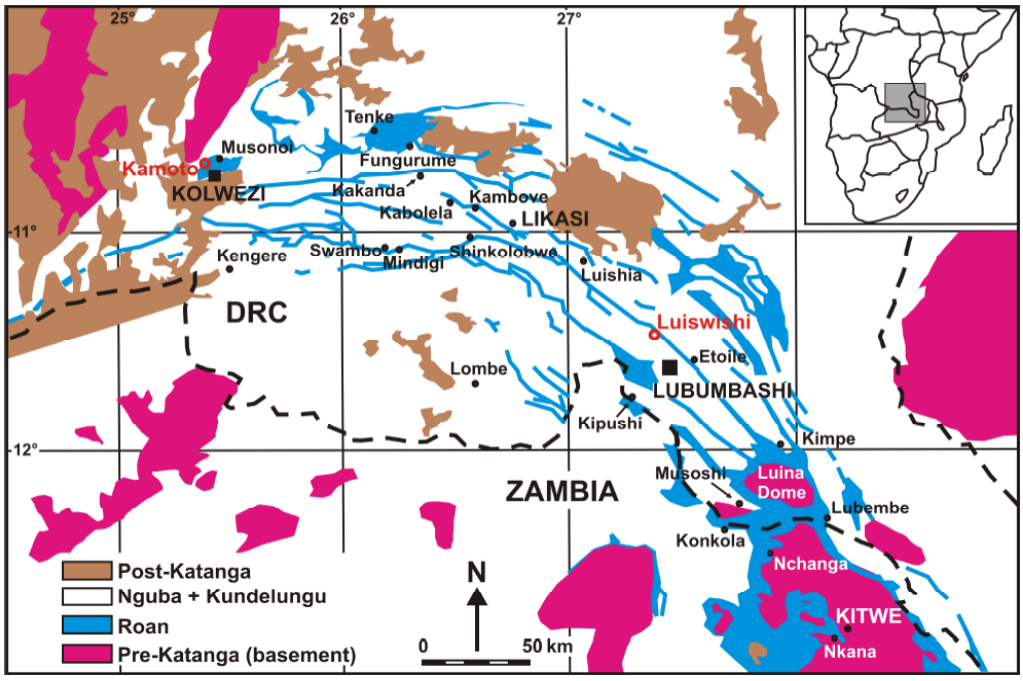

Figure 1. Geologic map of the Central African Copperbelt showing the location of the Luiswishi and Kamoto deposits. Originally from François (1973), adapted by Cailteux (1994) and El Desouky et al. (2009).

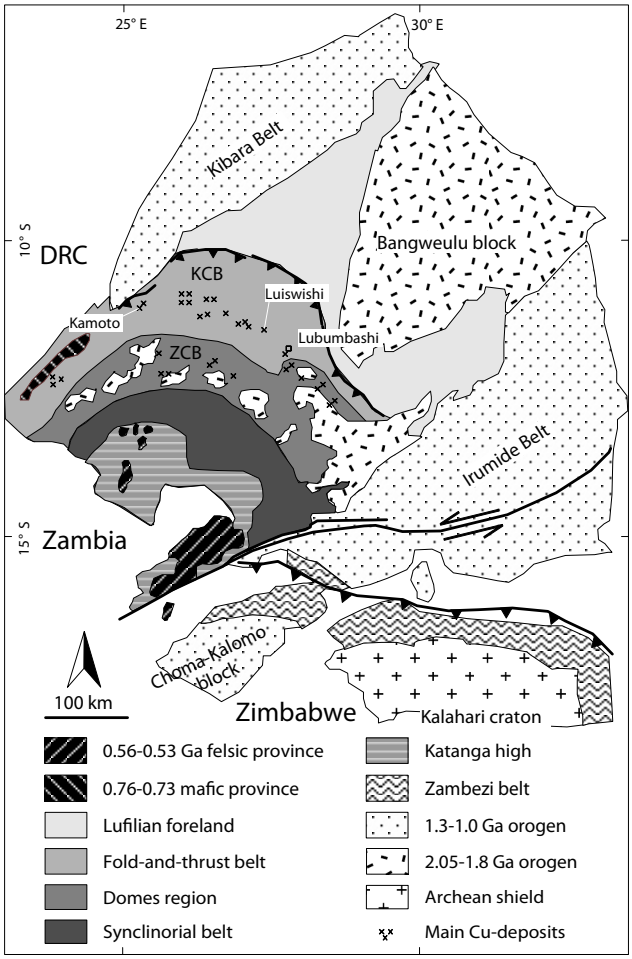

Figure 2. Map showing the different tectonic zones in the Lufilian Fold-and-Thrust Belt, from south to north, the Katanga High, the Synclinorial Belt, the Domes Region and the External Fold-and Thrust Belt. The latter hosts the Luiswishi and Kamoto deposits. The distribution of the Copperbelt deposits and the position of the Katanga Copperbelt (KCB) and the Zambian Copperbelt (ZCB) are also indicated. From Kampunzu & Cailteux (1999), modified by Porada & Berhorst (2000), De Waele et al. (2006) and Kipata (2013).

from a continental rift basin to a Red Sea-type proto-ocean with predominantly dolomitic shales in the Upper Roan and the overlying Nguba Group (Clemney, 1974). Convergence between the Congo and Kalahari cratons during the Lufilian Orogeny between 590 and 530 Ma (Rainaud et al., 2005) resulted in closing of this basin, folding and predominantly northward displacement of nappes, generating the Lufilian Fold-and-Thrust belt, currently present as a northward convex arcuate belt straddling the border between Zambia and the DRC. From south to north, this belt is subdivided in four distinct tectonic zones (e.g. Selley et al., 2005): (1) the Katanga High, (2) the Synclinorial Belt, (3) the Domes Region and (4) the External Fold-and-Thrust Belt (Fig. 2). This paper focuses on the Katangan part of the Copperbelt situated in the External Fold-and-Thrust Belt (EFTB). The EFTB is characterized by thin-skinned tectonics with macroscale fragmentation and repeated stacks of the Katanga Supergroup along thrust faults. Except for the basal Nzilo conglomerate, all exposed Roan deposits in the DRC are therefore allochtonous (Cailteux et al., 2007). At Luiswishi, in the southeastern part of the Katanga Copperbelt (Fig. 1), the mineralization occurs within a discordant megabreccia in a tightly folded syncline (Cailteux et al., 2003). The occurrence of secondary enrichment through supergene reworking is evidenced by the occurrence of malachite-, chrysocolla- and heterogenite-dominated deposits (Decrée et al., 2010; De Putter et al., 2010). The Kamoto deposit is located in the so-called Kolwezi megabreccia klippe, a 10 by 20 km erosional remnant of a thrust sheet emplaced in the northwestern part of the Katanga Copperbelt (François, 1974; Decrée et al., 2011).

2.2 Stratigraphy

The Katanga Supergroup is traditionally subdivided into the Roan, the Nguba and the Kundulungu Groups, which are separated by regionally extensive glacial diamictites (e.g. François, 1974; Cailteux et al., 2005b). In the DRC, the Roan Group is further subdivided in the Roches Argillo-Talqueuses (R-1, RAT), the Mines (R-2), the Dipeta (R-3) and the Mwashya (R-4) Subgroup (Cf. Fig. 3 for a detailed overview). In spite of their name, unweathered Roches Argillo-Talqueuses units are devoid of talc (Cailteux et al., 2005a) and consist dominantly of chlorite, dolomite and quartz. The aptly named Mines Subgroup hosts the majority of economic mineralization and comprises an alternation between dolomites and organic-rich argillaceous

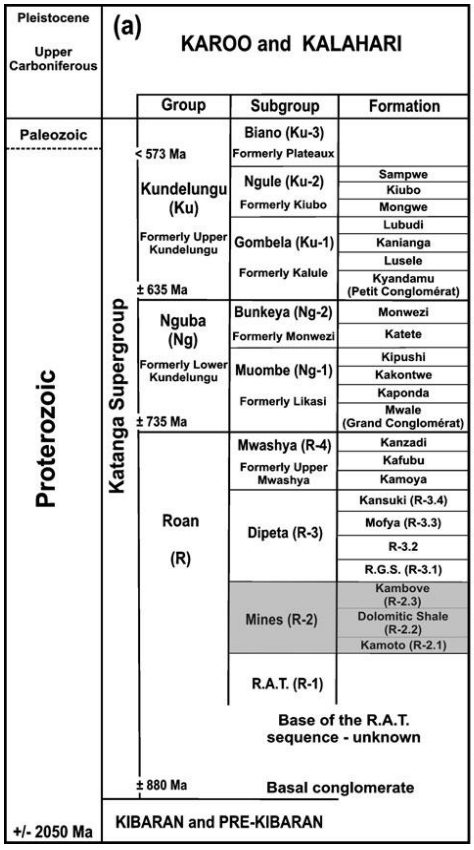

(b)

Formation	Member	Ore	Com. thick. (m)	Lo. thick. at Ls. (m)
Kambove (R-2.3) (Formerly C.M.N.) (up to 190m thick)	Upper Kambove (R-2.3.2) (Formerly Upper Calcaire à Minerai Noir or Upper C.M.N.)		40-100	not represented
	Lower Kambove (R-2.3.1) (Formerly Lower Calcaire à Minerai Noir or Lower C.M.N.)	Third Orebody (Lenses)	60-90	5.6-19.3
Dolomitic Shale (S.D.; R-2.2) (up to 140m thick)	S.D.-3b		30-125	13.1-31.7
	S.D.-3a			
	S.D.-2d			
	S.D.-2c			
	S.D.-2b			
	S.D.-2a			
	Black Ore Mineralized Zone (B.O.M.Z.; S.D.-1b)	Upper Orebody	5-15	1.7-7.4
	Shales Dolomitiques de Base (S.D.B.; S.D.-1a)			
Kamoto (R-2.1) (up to 50m thick)	Roches Siliceuses Cellulaires (R.S.C.)		0-30	1-4.3
	Roches Siliceuses Feuilletées (R.S.F.)	Lower Orebody	6-12.5	2.1-9
	Dolomites Stratifiées (D.Strat.)			
	Roches Argilo Talqueuses grises (gray R.A.T.)		0.5-5	3.9-8.1

Figure 3. Stratigraphic subdivisions of the Katanga Supergroup and radiometric ages. In the Mines Subgroup, common thicknesses and local thickness at Luiswishi are reported (comm. Thick and Lo thick. respectively). After François (1973, 1987), modified by a.o. Cailteux (1994), Cailteux et al. (2007), Batumike et al. (2007) and El Desouky et al. (2009).

dolomites and siltstones, subdivided in the Kamoto (R-2.1), Dolomitic Shale (R-2.2) and the Kambove (R-2.3) Formations. Ore deposits occur at three stratigraphic intervals separated by poorly mineralized or barren zones: (1) the Lower Orebody in the Kamoto Formation (R-2.1), (2) the Upper Orebody at the base of the Dolomitic Shale Formation (R-2.2, SD) and (3) discontinuous intervals in the Third Orebody in the lower part of the Kambove Formation (R-2.3).

2.3 Cu-Co mineralization

Mineralogically and texturally, the Cu-Co mineralization in the Kamoto and Luiswishi deposits are similar (e.g. Dewaele et al., 2006; El Desouky et al., 2009, 2010). Early diagenetic framboidal pyrite and widespread dolomitization predates the main Cu-Co mineralization of chalcopyrite, bornite, carrollite and chalcocite (Dewaele et al., 2006; Muchez et al., 2008). Gangue material is mostly dolomite and quartz with some accessory Mg-chlorite and muscovite (El Desouky et al., 2009; Fontaine et al., 2010). At Kamoto, Dewaele et al. (2006) recognized four generations of dolomite cement using cathodoluminescence. In this deposit carrrolite, digenite, bornite and chalcocite dominate the Lower and Upper Orebodies whereas the presence of pyrite and chalcopyrite is restricted to the upper part of the Upper Orebody (Dewaele et al., 2006).

El Desouky et al. (2009) described four different mineralization textures and occurrences: (1) disseminated fine- or coarse-grained sulfides, individual or in aggregates; (2) fine and coarse-grained sulfides in individual nodules and layers; (3) coarse-grained sulfides in mm- to dm-thick massive veins and finally (4) coarse-grained sulfides in cm- to m-scale tectonic breccia cement. Fine-grained Cu-Co sulfides coexist with quartz replacing dolomite, while coarser grained sulfides are associated with dolomite overgrowing and partially replacing quartz. Pyrite is replaced by chalcopyrite, which is in turn replaced by bornite and finally chalcocite replaces bornite, consistent with the paragenetic sequence predicted by reactive transport modeling (Muchez & Corbella, 2012). Supergene minerals comprise, among other, chalcocite, digenite and covellite, malachite, heterogenite, azurite, chrysocolla, hematite and limonite (El Desouky et al., 2009, 2010; De Putter et al., 2010).

Fluid inclusion studies revealed distinct mineralizing fluids, inferred to represent at least two main mineralization phases (El Desouky et al., 2009, 2010). The first stratiform Cu-Co mineralization formed at temperatures between 115 and 200 °C, from moderately saline mineralizing fluids (11.3-20.9 eq. wt% NaCl). The second, synorogenic stratiform to stratabound Cu-Co mineralization phase is linked with a highly saline (35-45.5 eq. wt% NaCl), hot (270-385 °C) mineralizing fluid (El Desouky et al., 2009). Although the second phase has not been dated, it is thought to be contemporaneous with the Lufilian Orogeny (e.g. El Desouky et al., 2010), which started at ca. 590 Ma and culminated around ca. 530 Ma (Rainaud et al., 2005). The second phase of Cu-Co mineralization is thought to rework the mineralization from the first phase, because of its similar mineralogy and the preservation of a dominantly bacterially reduced sulfur component (El Desouky et al., 2009, 2010). All samples studied belong to the second mineralization phase.

3. Methodology

Fresh, unweathered dolomite samples from cores LSW1215, LSW1216, LSW1301 at Luiswishi and F120 at Kamoto (identical samples were studied by El Desouky et al., 2009, 2010) were analyzed. Dolomite and quartz form the main, ubiquitous gangue minerals. Since the REY content in quartz is negligible, the REY concentration of the gangue dolomites is measured. A diamond-tipped drill was used to sample ±0.1 g of gangue dolomite taking care to avoid sulfides, clay or carbonate particles from the surrounding host rocks. This dolomite was subsequently dissolved with 1 ml 6 M HCl, while heating in a warm water bath for 2 hours at 80 °C. The acid-insoluble fraction did not exceed 2 wt%, except in KH05 and KH15 (69 and 18 wt% respectively) and is almost exclusively composed of quartz, the other main gangue mineral phase. The obtained sample digests were subsequently diluted to 50 ml with Milli-Q (18.2 MΩ·cm), spiked with internal standards (In and Re; both 5 µg L^{-1}) and analyzed with a Perkin-Elmer SCIEX Elan DRC*Plus* single-collector ICP-MS instument at Ghent University. International rock reference standards GBW7114, DWA-1, CCH-1 (carbonates with variable clay content) and basalt BCR-1 were included in the measuring sequence and calibration was performed via external calibration versus a set of multi-element standard solutions with concentrations ranging between 1 and 20 µg L^{-1} (prepared by appropriate dilution of a 0.1 g L^{-1} commercially available REY multi-element standard solution). Oxide and hydroxide ratios were determined for the light REE, by measuring separate sets of multi-element standard solutions under identical measuring conditions (in order to be able to determine the signals for X^+, XO^+ and XOH^+ interference-free). In this way, possible spectral overlap of REE-signals with those of oxides or hydroxides of the low REE can be corrected for. Geo-reference standards GBW7114, DWA-1, CCH-1 and BCR-1 were dissolved with microwave-assisted dissolution (HF-HNO_3-$HClO_4$), while GBW7114 and two in-house carbonate standards namely dolomite from the black ore mineralized zone or BOMZ from Kambove and pure calcite of unknown origin from the mineral collection at the Geo-institute, KU Leuven were dissolved according to the same HCl procedure used on the dolomite samples studied. The reference composition of the in-house standards was constrained by three repeated ICP-MS measurements of Li-borate fluxed samples performed by Actlabs (Torremans, 2011). The REE concentrations obtained from both the HCl- and the microwave-assisted dissolution procedure are in good agreement with the reference values. The Y-recovery was only 88 ±2% (1s, n=6), likely because the

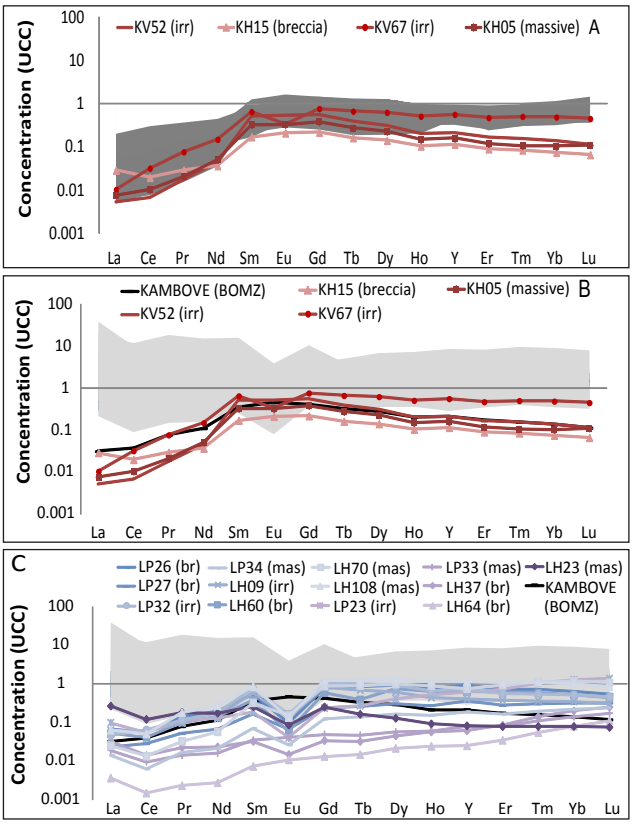

Figure 4. Upper Continental Crust (UCC)-normalized REY-composition of the Kamoto dolomites (A) and (B) and REY patterns at Luiswishi (C). In (C), Type I patterns and Type II patterns (see 4.) correspond to blue and light purple shades respectively. The dark grey shaded area in Fig4A corresponds to the main range of hydrothermal carbonate composition reported by Wagner et al. (2010), whereas the grey shaded area (B) and (C) shows the composition range of the host rocks, compiled from De Putter et al. (2010), Torremans (2011) and own data. The Kambove BOMZ (black ore mineralized zone) is a host rock sample, depleted in LREE and HREE compared to the BOMZ samples analyzed by De Putter et al. (2010). Abbreviations: massive vein (mas), irregular vein (irr), breccia cement (br). UCC composition after Rudnick & Gao (2003).

Table 1. Petrographic description, core ID and depth to surface of the samples analyzed for their REY content. In figures and in the text, the sample IDs listed are abbreviated to the format displayed in the second column. See Fig. 3 for the abbreviations of the stratigraphic units.

Sample ID	Tag	Host rock	Drill core	Depth (m)	Description
KA07HA05	KH05	D strat	F120	64.7-67	massive vein with dolomite quartz and chalcocite/carrollite
KA07HA15	KH15	RSC	F120	75.7	breccia cement, 5 mm thick dolomite, quartz and minor apatite, sulfides oxidized
KA05VD52	KV52	RSF	F120	73.0	irregular vein crosscutting chertified host rock with layer-parallel bands and lenticules with dolomite, quartz and chalcocite/carrollite
KA05VD67	KV67	SD1a	F120	98.0	irregular vein (3 cm thick), sulfides oxidized
LS06HA09	LH09	SD3a	LSW1215	52.1	irregular vein, boudinaged, coarse-grained with chalcopyrite (<3mm thick)
LS06HA23	LH23	BOMZ	LSW1215	80.3	massive, 1 cm thick dolomite core surrounded by 4 cm quartz and a few cm-sized apatite grains, rimmed by chalcopyrite
LS06HA37	LH37	RSF	LSW1216	120.9	breccia cement with dolomite, quartz and chalcopyrite, coarse-grained
LS06HA60	LH60	L-CMN	LSW1216	172	breccia cement with dolomite and chalcopyrite, slightly ferrous
LS06HA64	LH64	SD2a	LSW1216	185.2	breccia cement, mostly ferrous, with dolomite and chalcocite, non-ferrous central part drilled
LS06HA70	LH70	SDB	LSW1216	192.4	irregular vein with dolomite and chalcopyrite rim, 7 mm wide, central part drilled
LS06HA108	LH108	Gray RAT	LSW1301	144.4	massive vein with quartz, dolomite and chalcopyrite
LS11PM23	LP23	RSF	LSW1216	121.1	irregular vein with quartz, dolomite, chalcopyrite and accessory apatite
LS11PM26	LP26	CMN	LSW1216	172.2	breccia cement consisting of dolomite, quartz and chalcopyrite
LS11PM27	LP27	SD2a	LSW1216	184.7	breccia cement consisting of dolomite, quartz, chalcocite, chalcopyrite and accessory apatite
LS11PM32	LP32	SD3a	LSW1215	52.0	irregular vein with quartz, dolomite, chalcopyrite and minor apatite
LS11PM33	LP33	BOMZ	LSW1215	80.4	massive vein with quartz ,dolomite, chalcopyrite and minor apatite
LS11PM34	LP34	SDB/ RSC	LSW1215	82.4	massive vein with quartz, dolomite, chalcopyrite and accessory apatite

Sample ID	Type	La	Ce	Pr	Nd	Sm	Eu	Gd	Tb	Dy	Ho	Y	Er	Tm	Yb	Lu
KA07HA05	massive vein	0.24	0.66	0.15	1.38	1.54	0.33	1.53	0.19	0.89	0.13	3.37	0.28	0.03	0.21	0.03
KA07HA15	breccia cement	0.90	1.25	0.21	0.99	0.81	0.21	0.88	0.11	0.55	0.09	2.42	0.21	0.03	0.15	0.02
KA05VD52	irregular vein	0.36	0.94	0.28	2.73	5.43	1.18	4.92	0.62	2.68	0.38	9.93	0.87	0.10	0.62	0.08
KA05VD67	irregular vein	0.32	2.03	0.55	4.04	3.08	0.33	3.07	0.47	2.45	0.42	11.82	1.09	0.15	0.98	0.14
LS06HA09	irregular vein	1.87	3.60	0.68	3.88	2.71	0.13	3.18	0.48	2.38	0.36	8.39	0.84	0.11	0.69	0.09
LS06HA23	massive vein	8.08	7.43	1.27	4.59	1.18	0.08	0.99	0.11	0.49	0.07	1.69	0.18	0.02	0.15	0.02
LS06HA37	breccia cement	0.98	0.86	0.16	0.61	0.15	0.01	0.13	0.02	0.17	0.05	1.25	0.19	0.04	0.39	0.08
LS06HA60	breccia cement	1.56	2.55	0.70	3.69	1.75	0.06	2.31	0.26	2.82	0.52	12.91	1.36	0.17	1.01	0.14
LS06HA64	breccia cement	0.11	0.09	0.02	0.07	0.03	0.01	0.05	0.01	0.08	0.02	0.51	0.08	0.02	0.16	0.03
LS06HA70	massive vein	0.79	0.86	0.24	1.58	1.55	0.15	3.57	0.65	3.95	0.76	16.32	2.18	0.34	2.40	0.34
LS06HA108	massive vein	1.92	3.10	1.24	7.25	3.87	0.13	4.82	0.84	5.06	0.93	23.65	2.44	0.33	1.99	0.25
LS11PM23	irregular vein	3.00	3.34	0.80	3.36	0.87	0.04	0.92	0.19	1.58	0.42	12.46	1.61	0.31	2.50	0.41
LS11PM26	breccia cement	2.03	3.54	0.98	5.18	2.50	0.09	3.07	0.57	3.52	0.65	19.10	1.65	0.21	1.24	0.16
LS11PM27	breccia cement	0.71	1.74	0.36	1.79	0.76	0.07	0.93	0.18	1.16	0.22	7.49	0.63	0.09	0.62	0.10
LS11PM32	irregular vein	1.42	4.00	0.81	4.84	3.52	0.16	4.18	0.68	3.50	0.54	15.15	1.26	0.16	1.02	0.14
LS11PM33	massive vein	0.58	0.59	0.10	0.43	0.16	0.04	0.19	0.03	0.22	0.05	1.63	0.18	0.03	0.28	0.05
LS11PM34	massive vein	0.43	0.39	0.11	0.56	0.32	0.03	0.48	0.09	0.62	0.13	3.89	0.37	0.06	0.43	0.07

Sample ID	Type	∑REE	La_N/Lu_N	La_N/Sm_N	Dy_N/Yb_N	Tb_N/Lu_N	Ce/Ce*	Pr/Pr*	Eu/Eu*
KA07HA05	massive vein	7.59	0.07	0.02	2.20	2.48	0.72	0.69	0.93
KA07HA15	breccia cement	6.40	0.44	0.17	1.89	2.46	0.68	1.04	1.08
KA05VD52	irregular vein	21.20	0.05	0.01	2.22	3.46	0.58	0.68	0.99
KA05VD67	irregular vein	19.12	0.02	0.02	1.28	1.48	0.74	0.85	0.47
LS06HA09	irregular vein	20.99	0.20	0.10	1.78	2.31	0.73	0.95	0.20
LS06HA23	massive vein	24.68	3.57	1.04	1.63	2.18	0.54	1.24	0.33
LS06HA37	breccia cement	3.85	0.13	1.01	0.23	0.13	0.51	1.22	0.45
LS06HA60	breccia cement	18.89	0.12	0.14	1.43	0.87	0.54	1.12	0.12
LS06HA64	breccia cement	0.78	0.03	0.50	0.26	0.13	0.50	1.09	1.05
LS06HA70	massive vein	19.36	0.02	0.08	0.85	0.84	0.46	0.92	0.25
LS06HA108	massive vein	34.17	0.08	0.08	1.30	1.46	0.42	1.10	0.13
LS11PM23	irregular vein	19.35	0.07	0.52	0.32	0.20	0.51	1.27	0.19
LS11PM26	breccia cement	25.39	0.12	0.12	1.46	1.55	0.55	1.11	0.14
LS11PM27	breccia cement	9.34	0.07	0.14	0.97	0.81	0.75	1.08	0.33
LS11PM32	irregular vein	26.22	0.10	0.06	1.76	2.14	0.80	0.93	0.18
LS11PM33	massive vein	2.93	0.11	0.55	0.40	0.27	0.57	1.10	0.96
LS11PM34	massive vein	4.09	0.06	0.20	0.74	0.59	0.41	1.21	0.27

Table 2. Acid-soluble REY composition (in µg g^{-1}) of the Kamoto and Luiswishi carbonates analyzed. The table includes the Upper Continental Crust (UCC)-normalized La/Lu, La/Sm, Dy/Yb and Tb/Lu ratios, the sum of the REE concentrations (∑REE, in ppm) and finally the Ce, Pr and Eu anomalies with respect to the UCC (Ce/Ce*, Pr/Pr* and Eu/Eu* respectively), wherein Ce, Pr and Eu are the UCC-normalized concentrations and Ce*, Pr* and Eu* are calculated as the arithmetic mean of the UCC-normalized La and Pr, Ce and Nd, and Sm and Gd concentrations respectively. UCC composition after Rudnick & Gao (2003).

atomic mass of Y (atomic mass 88.9 g/mol) falls below the mass range bracketed by the internal standards. The Y-values were therefore corrected to match the standard reference values. The performed oxide corrections had no significant effect on the REE concentrations, except for a very small barium(hydr)oxide overlap on Eu.

4. Results

The samples analyzed belong to the synorogenic mineralization phase and comprise dolomitic breccia cement, irregular mineralization and massive veins. Petrographic descriptions, borehole ID and depth to surface can be found in Table 1, while the results from the chemical analysis are presented in Table 2, wherein all ratios are reported as Upper Continental Crust (UCC)-normalized ratios, using the UCC composition from Rudnick & Gao (2003). This study elects to present and discuss the REY data with respect to the UCC reference frame. In Fig. 4, the REY patterns are presented in three groups: Kamoto dolomites with respect to typical hydrothermal carbonates (Fig. 4A), Kamoto dolomites and their host rocks (Fig. 4B) and Luiswishi dolomites and their host rocks (Fig. 4C).

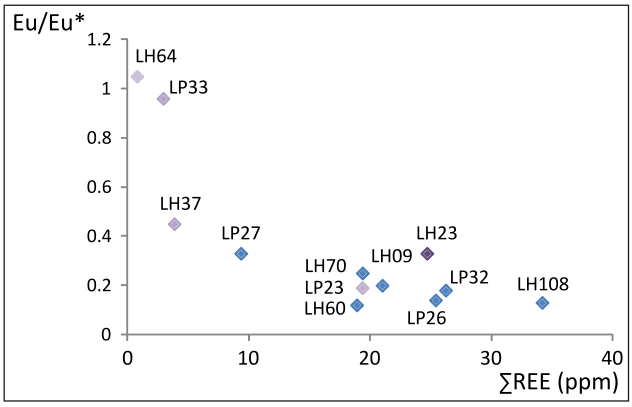

Figure 5. Eu/Eu* versus ∑REE plot showing the correlation between the UCC-normalized Eu anomaly and the total REE concentration for the Luiswishi dolomites (∑REE, in µg g^{-1}). Type I patterns and Type II patterns (see 4.) are represented by blue and light purple diamonds respectively.

The host rocks display highly variable patterns which are either slightly LREE depleted, UCC-like or (extremely) LREE enriched compared to the UCC, with normalized concentrations mostly between 0.3 and 7, although some host rocks contain LREE concentrations up to ~40 times the UCC-content. Most are characterized by relatively flat MREE-HREE patterns mainly ranging between 0.15 and 3 times the UCC composition.

The gangue dolomites from Kamoto (Fig. 4A and 4B) display depleted REE-patterns with total REE concentration (∑REE) ranging between 6 and 21 ppm and La_N/Lu_N ratios between 0.02 and 0.07, except in the breccia (0.44), which shows an elevated LREE content. The UCC-normalized LREE and HREE concentrations are lower than the MREE content, resulting in a convex-upward REY pattern centered on Eu. Such convex-upward UCC-normalized REY patterns with an apparent MREE enrichment are commonly observed in high temperature hydrothermal fluids (Fig.. 4A; Lüders et al., 1993; Hecht et al., 1999; Allwood et al., 2010).

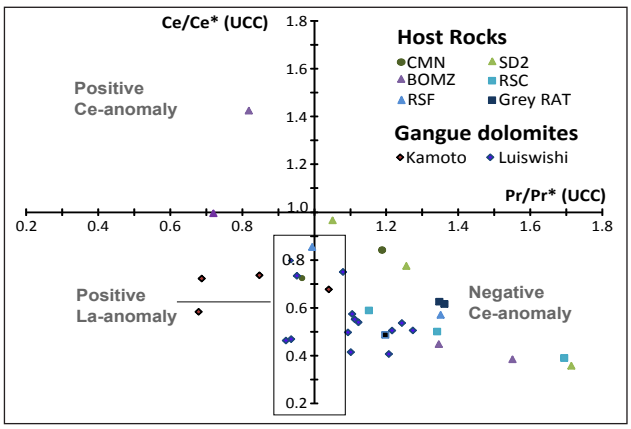

Figure 6. Ce-Pr diagram from Bau & Dulski (1996): Ce* and Pr* are calculated as the arithmetic mean of the UCC-normalized La and Pr, and Ce and Nd concentrations respectively. Originally designed to distinguish between Ce anomalies and positive La anomalies (defined as the field indicated on the graph) in marine carbonates. Host rocks data from De Putter et al. (2010), Torremans (2011) and own data. UCC composition after Rudnick & Gao (2003).

Apart from massive vein LH23, all Luiswishi dolomites are depleted in LREE compared to their respective UCC-normalized MREE and HREE content (Fig. 4C). Their total REE content ranges between 0.8 and 34 ppm with an average La_N/Lu_N ratio of 0.10. Two general types of patterns are observed at Luiswishi. Type I patterns display a pronounced LREE-MREE fractionation (La_N/Sm_N 0.06-0.20), followed by near-flat to slightly decreasing MREE-HREE patterns (Fig. 4C, blue shades). They are reminiscent of the Kamoto patterns, although the MREE-HREE fractionation is slightly less pronounced, as indicated by their Dy_N/Yb_N ratio between 0.85 and 1.78 compared to 1.28-2.22 at Kamoto. Type II patterns (LP23, LP33, LH37, LH64) are characterized by a relatively small LREE-MREE fractionation (La_N/Sm_N 0.50 - 1.01) associated with a pronounced MREE-HREE enrichment (Dy_N/Yb_N 0.26 - 0.32 by Fig. 4C, light purple shades). Their La_N/Lu_N ratios are similar to those in the Type I veins (average 0.09). Massive dolomite LH23 (Fig.4C, dark purple) shows a flat LREE-MREE pattern followed by a gradual MREE-HREE depletion which fits neither pattern type.

Eu anomalies are absent at Kamoto, except in the irregular vein (KV67) that shows the highest REE-concentrations. In contrast, most Luiswishi dolomites show pronounced negative Eu anomalies (Eu/Eu* 0.12-0.45), with the exception of a massive vein (LP33) and a breccia cement (LH64). Furthermore, there is a significant correlation between the total REE concentration (∑REE) and the size of the Eu anomaly at Luiswishi (Fig. 5). While the slope of a linearly decreasing trend is significantly different from zero at the 99.7 % confidence level, this trend is associated with a relatively low correlation coefficient (r^2) of 0.66, indicating a large amount of residual variation not explained by this trend.

The Ce-Pr diagram from Bau & Dulski (1996) is used to distinguish between La and Ce anomalies (Fig. 6). The analyzed host rocks often show pronounced negative Ce and Eu anomalies (Fig. 6; De Putter et al., 2010). The Kamoto dolomites show low Pr/Pr* values indicative for positive La anomalies rather than real negative Ce anomalies, with the exception of breccia KH15. All Luiswishi dolomites show Ce/Ce* ratios below unity, which combined with the elevated Pr/Pr*-ratios in most samples indicates a negative Ce anomaly. Dolomites LH09, LH67, LH70 and LP32 also show Pr/Pr* ratios below unity indicating positive La anomalies (Fig. 6).

5. Discussion

The Cu-Co mineralizing fluids in the Copperbelt are thought to leach their metals from the basement and/or the overlying siliciclastics, after which interaction with reducing sediment layers rich in organic matter or with hydrocarbon reservoirs resulted in metal-sulfide precipitation (Annels, 1989; Selley et al., 2005; Muchez et al., 2008). To assess fractionation from the REY composition in the source, REY patterns are commonly normalized over the Post-Archean Australian Shale (PAAS) composition, which is then assumed to approximate the composition of the source (e.g. Roberts et al., 2009; Wagner et al., 2010). This study elects to normalize the REY data over the UCC composition (Rudnick & Gao, 2003), which is similar to PAAS, but results in less pronounced LREE depletions and lower Eu/Eu* values for the analyzed dolomites. Hydrothermal carbonates generally display normalized REY patterns with strongly depleted LREE, comparatively high MREE concentrations, a progressive decrease towards the HREE and near-chondritic Y/Ho ratios (e.g. Allwood et al., 2010; Wagner et al., 2010; Bons et al., 2012).

Mineralogical fractionation in hydrothermal calcite and dolomite appears to be relatively minor and therefore it can be assumed that the dolomite composition approximates the composition of the fluid from which it precipitated (e.g. Zhong & Mucci, 1995; Hecht et al., 1999; Roberts et al., 2009). The apparent MREE enrichment is traditionally explained by a combination of HREE retention in resistant source rock minerals (e.g. zircon) with complexation-driven LREE depletion (e g. Lüders et al., 1993; Hecht et al., 1999). However, recent experimental studies (Migdisov et al., 2009) have shown that at elevated temperatures, Cl^- and F^- preferentially complexate the LREE. Both Cl^- and F^- are inferred to be important REE-ligands in hydrothermal brines (Bach et al., 2003; Kučera et al., 2009), especially at higher temperatures (Migdisov & Williams-Jones, 2007), and therefore, complexation-driven fractionation is unlikely to explain the observed LREE depletion. Furthermore, the magnitude of the LREE depletion precludes a direct inheritance of the source and therefore, the LREE depletion likely resulted from precipitation of one or more LREE-selective mineral phases. Minerals that preferentially incorporate LREE and which have been reported from Kamoto or Luiswishi are chlorite and chalcocite, the latter of which may contain more than 300 ppm of La and Ce and a La_N/Yb_N ratio close to 30 (De Putter et al., 2010). Elevated La_N/Lu_N ratios in some samples both at Kamoto (e g., in breccia cement KH15) and Luiswishi can in principle be explained through interaction with their host rock (carbonate). Sr isotope data indeed suggests that the Sr of the second mineralization phase at Kamoto and Luiswishi ($^{87}Sr/^{86}Sr_{530Ma}$ 0.70881-0.71135) can largely be buffered by the host rock carbonates ($^{87}Sr/^{86}Sr_{530Ma}$ 0.70698-0.70903) rather than by the felsic basement ($^{87}Sr/^{86}Sr_{530Ma}$ 0.72201-0.78745) which has a much more radiogenic Sr signature (Nyogi et al., 1991; El Desouky et al. 2010). However, mass balance considerations and Sr-Nd isotope studies illustrate that REY-buffering is much more unlikely compared to Sr-buffering in hydrothermal carbonate systems (e.g. Banner et al., 1988; Barker et al., 2009).

At Luiswishi, ramp-shaped Type I or 'linearly' increasing Type II REY patterns occur seemingly independent of the stratigraphic position, depth to surface, host rock or morphology (irregular, massive mineralization or breccia cement). The difference between both types indicates a distinct difference in physicochemical conditions in the brines and/or source composition at this deposit. The temperature of the synorogenic fluids at Luiswishi, as indicated by fluid inclusion studies, ranges between 300 °C and 385 °C compared to 270-320 °C at Kamoto (El Desouky et al., 2009). The latter is consistent with a relatively minor metamorphic overprint inferred for Kamoto (Bartholomé et al., 1972; Bartholomé, 1974) and hence more intense metamorphic conditions at Luiswishi are expected to contribute to the differences with the Kamoto deposit.

The presence of positive Eu anomalies is also a characteristic feature of hydrothermal carbonates and is commonly explained by less efficient sorption and differences in complexation behavior between divalent Eu and the trivalent REE (e.g. Allwood et al., 2010). However, positive Eu anomalies with respect to the UCC are absent at Kamoto, whereas they are prominent in other hydrothermal carbonates (e.g. Wagner et al., 2010; Eu/Eu* 1.20-1.82). These comparatively small Eu/Eu*-values likely relate to the oxidizing conditions inferred for the Copperbelt brines wherein Eu is not fractionated from the other REE during brine transport.

The large negative Eu anomalies at Luiswishi are either inherited from the sources, generated during brine transport or through remobilization during the second mineralization stage. The association of these negative Eu anomalies with high total REY contents (Fig. 5) are in favor of the latter interpretation. Under the reducing conditions at the sites of mineralization, Eu is likely reduced to fluid-mobile, divalent Eu and therefore preferentially lost to the fluid during subsequent remobilization. In this context, the absence of Eu anomalies in the REY-poor breccia cement LH64 and in massive vein LP33 is explained by less remobilization from the mineralized rocks, resulting in a REY signature more characteristic for the pristine fluid. The presence of both Ce and Eu anomalies at Luiswishi can be explained by changing redox conditions during fluid migration, mineral precipitation and later recrystallization or by inheritance from the source rocks or marine fluids (e.g. Lüders et al., 1993; Roberts et al., 2009). If Ce is (partly) tetravalent in the oxidizing mineralizing brines, it is most likely depleted with respect to the trivalent REE (Brookins, 1988).

6. Conclusion

While the stratiform to stratabound Cu-Co deposits at Kamoto and Luiswishi display similar ore mineralogy, paragenesis, textural characteristics and their host rocks are lateral stratigraphic equivalents, the REY-signature of gangue dolomites from the

second main mineralization phase is remarkably different. Most features of the Kamoto dolomites and (to a lesser extent) Type I Luiswishi dolomites are typical for hydrothermal carbonates (e.g. Wagner et al., 2010). The LREE depletion most likely results from fractionation of a LREE-selective mineral phase, while the progressive depletion from MREE to HREE likely results from HREE retention in the sources (Lüders et al., 1993). The presence of ramp-shaped Type I patterns and 'linearly' increasing Type II patterns at Luiswishi indicates distinct difference in physicochemical conditions in the brines and/or source composition at this deposit. More intense metamorphic conditions during synorogenic mineralization at Luiswishi (Bartholomé et al., 1972; Bartholomé, 1974; El Desouky et al., 2009) are expected to contribute to the differences with the Kamoto deposit. The increased LREE content in some samples is indicative for a (minor) REY contribution from the host rocks. Unlike most Kamoto dolomites, the Luiswishi dolomites generally display pronounced negative Eu anomalies which correlate with their total REE content. The latter is taken to reflect Eu-depletion during remobilization, while the residual variation reflects the influence of variable physicochemical conditions in the brine and/or differences in source composition.

7. Acknowledgments

We thank the Forrest International Group and especially dr. ir Jacques Cailteux for the permission to study and sample the Luiswishi boreholes. We are grateful to dr. Hamdy El Desouky, Prof. Jan Hertogen, dr. Elvira Vassilieva, dr. Stijn Dewaele and drs. Jorik Van Wilderode for stimulating discussions on various subjects. This paper benefited greatly from helpful and constructive comments by dr. Thierry De Putter, an anonymous reviewer and from editorial handling by Prof. Jean-Clair Duchesne. David Debruyne and Lieve Balcaen are respectively Research Assistant and Senior Research Assistant of the Fund for Scientific Research – Flanders (FWO-Vlaanderen). This research is also financially supported by the research grant G.A078.11 from FWO-Vlaanderen (Belgium).

8. References

Annels, A.E., 1989. Ore genesis in the Zambian Copperbelt with particular reference to the northern sector of the Chambishi basin. Geological Association of Canada, Special Paper, 36, 427-452.

Allwood, A.C., Kamber, B.S., Walter, M.R., Burch, I.W. & Kanik, I., 2010. Trace elements record depositional history of an Early Archean stromatolitic carbonate platform. Chemical Geology, 270(1), 148-163.

Armstrong, R.A., Master, S. & Robb, L.J., 2005. Geochronology of the Nchanga Granite, and constraints on the maximum age of the Katanga Supergroup, Zambian Copperbelt. Journal of African Earth Sciences, 42, 32-40.

Bach, W., Roberts, S., Vanko, D.A., Binns, R.A., Yeats, C.J., Craddock, P.R. & Humphris, S.E., 2003. Controls of fluid chemistry and complexation on rare earth element contents of anhydrite from the PACMANUS subseafloor hydrothermal system, Manus Basin, Papua New Guinea. Mineralium Deposita, 38, 916-935.

Banner, J.L., Hanson, G.N. & Meyers, W.J., 1988. Rare earth element and Nd isotopic variations in regionally extensive dolomites from the Burlington-Keokuk Formation (Mississippian); implications for REE mobility during carbonate diagenesis. Journal of Sedimentary Research, 58, 415-432.

Barker, S.L.L., Bennett, V.C., Cox, S.F., Norman, M.D. & Gagan, M.K.,, 2009. Sm–Nd, Sr, C and O isotope systematics in hydrothermal calcite–fluorite veins: Implications for fluid–rock reaction and geochronology. Chemical Geology, 268, 58-66.

Bartholomé, P., 1974. On the diagenetic formation of ores in sedimentary beds, with special reference to Kamoto, Shaba, Zaïre. In Bartholomé, P. (éd.), Gisements Stratiformes et Provinces Cuprifères. Centenaire de la Société Géologique de Belgique, Liége, 203-213.

Bartholomé, P., Evrard, P., Katekesha, F., Lopez-Ruiz, J., Ngongo, M., 1972. Diagenetic oreforming processes at Kamoto, Katanga, Republic of the Congo. In Amstutz, G.C., Bernard, A.J. (eds.), Ores in sediments. Springer-Verlag, Heidelberg, 21-41.

Bateman, A.M., 1930. Ores of the north Rhodesian Copperbelt. Economic Geology, 25, 365-418.

Batumike, M.J., Cailteux, J.L.H. & Kampunzu, A.B., 2007. Lithostratigraphy, basin development, base metal deposits, and regional correlations of the Neoproterozoic Nguba and Kundelungu rock successions, central African Copperbelt. Gondwana Research, 11, 432-447.

Bau, M. & Dulski, P,1996. Distribution of yttrium and rare-earth elements in the Penge and Kuruman iron-formations, Transvaal Supergroup, South Africa. Precambrian Research, 79, 37-55.

Bons, P.D., Elburg, M.A. & Gomez-Rivas, E., 2012. A review of the formation of tectonic veins and their microstructures. Journal of Structural Geology, 43, 33-62.

Brookins, D.G., 1988. Eh-pH diagrams for geochemistry. Springer, Berlin, 176.

Cailteux, J.L.H., 1994. Lithostratigraphy of the Neoproterozoic Shaba-type (Zaire) Roan Supergroup and metallogenesis of associated stratiform mineralization. Journal of African Earth Sciences, 19, 279-301.

Cailteux, J.L.H., Kampunzu, A.B., Ngoie Bwanga, F., 2003. Lithostratigraphy of the Mwashya Subgroup in Congo (central African Copperbelt), with special reference to the Luiswishi area. In Cailteux, J.L.H. (Org.), Proterozoic Sediment- Hosted Base Metal Deposits of Western Gondwana., Abstract Volume of the Conference and Field Guidebook, 3rd IGCP-450 Meeting and Field Workshop, Lubumbashi, D.R.Congo, 83-88.

Cailteux, J.L.H., Kampunzu, A.B.H. & Batumike, M.J., 2005a. Lithostratigraphic position and petrographic characteristics of R.A.T. ('Roches Argilo-Talqueuses') Subgroup, Neoproterozoic Katangan Belt (Congo). Journal of African Earth Sciences, 42, 82-94.

Cailteux, J.L.H., Kampunzu, A.B.H., Lerouge, C., Kaputo, A.K. & Milesi, J.P., 2005b. Genesis of sediment-hosted stratiform copper-cobalt deposits, central African Copperbelt. Journal of African Earth Sciences, 42, 134-158.

Cailteux, J.L.H., Kampunzu, A.B. & Lerouge, C., 2007. The Neoproterozoic Mwashya–Kansuki sedimentary rock succession in the central African Copperbelt, its Cu–Co mineralisation, and regional correlations. Gondwana Research, 11, 414-431.

Clemmey, H., 1974. Sedimentary geology of a late Precambrian copper deposit at Kitwe, Zambia. In Bartholomé, P. (éd.), Gisements stratiformes et provinces cuprifères. Centenaire de la Société Géologique de Belgique, Liège, 255-265.

Davidson, C.M., 1931. The geology and ore deposits of Chambishi, northern Rhodesia. Economic Geology, 26, 131-154.

Decrée, S., Deloule, E., Ruffet, G., Dewaele, S., Mees, F., Marignac, C., Yans, J. & De Putter, T., 2010. Geodynamic and climate controls in the formation of Mio-Pliocene world-class oxidized cobalt and manganese ores in the Katanga province. DR Congo. Mineralium Deposita, 45, 621-629.

Decrée S., Deloule É., De Putter T., Dewaele S., Mees F.,Yans J. & Marignac, C., 2011. SIMS U–Pb dating of uranium mineralization in the Katanga Copperbelt: Constraints for the geodynamic context. Ore Geology Reviews, 40, 81-89.

De Putter, T., Mees, F., Decrée, S. & Dewaele, S., 2010. Malachite, an indicator of major Pliocene Cu remobilization in a karstic environment (Katanga, Democratic Republic of Congo). Ore Geology Reviews, 38, 90-10

De Waele, B., Liégeois, J-P., Nemchin, A.A., Tembo, F., 2006. Isotopic and geochemical evidence of proterozoic episodic crustal reworking within the Irumide belt of south-central Africa, the southern metacratonic boundary of an Archaean Bangweulu Craton. Precambrian Research, 148,225-256.

Dewaele, S., Muchez, Ph., Vets, J., Fernandez-Alonzo, M. & Tack, L., 2006. Multiphase origin of the Cu–Co ore deposits in the western part of the Lufilian fold-and-thrust belt, Katanga (Democratic Republic of Congo). Journal of African Earth Sciences, 46, 455-469.

El Desouky, H.A., Muchez, P. & Cailteux, J., 2009. Two Cu–Co sulfide phases and contrasting fluid systems in the Katanga Copperbelt, Democratic Republic of Congo. Ore Geology Reviews, 36, 315-332.

El Desouky, H.A., Muchez, Ph., Boyce A.J., Schneider, J., Cailteux, J.L.H., Dewaele, S. & von Quadt, A., 2010. Genesis of sediment-hosted stratiform copper–cobalt mineralization at Luiswishi and Kamoto, Katanga Copperbelt (Democratic Republic of Congo). Mineralium Deposita, 45, 735-763.

Fontaine, L., Bernard, A. Cailteux, J., Decrée, S., De Putter T. & Yans, J., 2010. Mineralogical, petrographical and geochemical characterization of the weathered ores at Luiswishi Cu-Co quarry (Katanga, D.R. Congo). Poster presented at the International Symposium: The Quest for Natural Resources in Central Africa. The Case of the Mining Sector in DRC, Royal Museum for Central Africa, Tervuren, Belgium.

Fleischer, V.D., Garlick, W.G., Haldane, R., 1976. Geology of the Zambian Copper Belt. In Wolf, K.H. (ed.), Handbook of stratabound and stratiform ore deposits, 6, Elsevier, New York, 223-352.

François, A., 1973. L'extrémité occidentale de l'arc cuprifère shabien. Etude géologique. Bureau d'Etudes Géologiques, Gécamines-Exploitation, Likasi, Zaïre, 65 pp.

François, A., 1974. Stratigraphie, tectonique et minéralisations dans l'Arc cuprifère du Shaba (Rép.du Zaïre). In Bartholomé, P. (éd.), Gisements Stratiformes et Provinces Cuprifères, Centenaire de la Société Géologique de Belgique, Liège, 79-101.

François, A., 1987. Synthèse géologique sur l'Arc cuprifère du Shaba (Rép. du Zaïre). Société Belge de Géologie, Centenaire, 15-65.

Hecht, L., Freiberger, R., Gilg, H.A., Grundmann, G. & Kostitsyn, Y.A., 1999. Rare earth element and isotope (C, O, Sr) characteristics of hydrothermal carbonates: genetic implications for dolomite-hosted talc mineralization at Göpfersgrün (Fichtelgebirge, Germany). Chemical Geology, 155, 115-130.

Kampunzu, A.B. & Cailteux, J.L.H., 1999. Tectonic Evolution of the Lufilian Arc (Central Africa Copper Belt) during Neoproterozoic Pan African Orogenesis. Gondwana Research, 2, 401-421.

Kipata, L., 2013. Brittle tectonics in the Lufilian fold-and-thrust belt and its foreland. An insight into the stress field record in relation to moving plates (Katanga, DRC), PhD thesis, KU Leuven, 182 pp.

Kučera, J., Cempírek, J., Dolníček, Z., Muchez, P. & Prochaska, W., 2009. Rare earth elements and yttrium geochemistry of dolomite from post-Variscan vein-type mineralization of the Nízký Jeseník and Upper Silesian Basins, Czech Republic. Journal of Geochemical Exploration, 103, 69-79.

Lüders, V., Möller, P., Dulski, P., 1993. REE Fractionation in carbonates and fluorites. In Möller, P. & Lüders, V. (eds.), Formation of hydrothermal vein deposits. Monograph Series on Mineral Deposits, Bornträger, Berlin, 133-150.

Master, S., Rainaud, C., Armstrong, R.A., Phillips, D., Robb, L.J., 2005. Provenance ages of the Neoproterozoic Katanga Supergroup (Central African Copperbelt), with implications for basin evolution. Journal of African Earth Sciences, 42, 41-60.

McGowan, R.R., Roberts, S., Foster, R.P., Boyce, A.J. & Coller, D., 2003. Origin of the copper-cobalt deposits of the Zambian Copperbelt: An epigenetic view from Nchanga. Geology, 31, 497-500.

McGowan, R.R., Roberts, S., Boyce, A.J., 2006. Origin of the Nchanga copper–cobalt deposits of the Zambian Copperbelt. Mineralium Deposita, 40, 617-638.

Mendelsohn, F., 1961. Ore genesis: summary of the evidence. In Mendelsohn, F. (ed.), The geology of the Northern Rhodesian Copperbelt. Macdonald, London, 130-146.

Migdisov, A.A. & Williams-Jones, A.E., 2007. An experimental study of the solubility and speciation of neodymium (III) fluoride in F-bearing aqueous solutions. Geochimica et Cosmochimica Acta, 71, 3056-3069.

Migdisov, A.A., Williams-Jones, A.E. & Wagner, T., 2009. An experimental study of the solubility and speciation of the Rare Earth Elements (III) in fluoride- and chloride-bearing aqueous solutions at temperatures up to 300 °C. Geochimica et Cosmochimica Acta, 73, 7087-7109.

Misra, K.C., 2000. Understanding mineral deposits. Kluwer Academic, Dordrecht, 845 pp.

Molak, B., 1995. Some structural and petrological aspects of the Cu (Co) mineralization in the Copperbelt and northwestern provinces of Zambia. Tervuren, Belgium, Royal Museum of Central Africa. Annales des Sciences Géologiques 101: 95-102.

Muchez, Ph., Vanderhaeghen, P., El Desouky, H., Schneider, J., Boyce, A., Dewaele, S. & Cailteux, J., 2008. Anhydrite pseudomorphs and the origin of stratiform Cu–Co ores in the Katangan Copperbelt (Democratic Republic of Congo). Mineralium Deposita, 43, 575-589.

Muchez, Ph., Brems, D., Clara, E., De Cleyn, A., Lammens, L., Boyce, A., De Muynck, D., Mukumba, W., Sikazwe, O., 2010. Evolution of Cu–Co mineralizing fluids at Nkana Mine, Central African Copperbelt, Zambia. Journal of African Earth Sciences, 58, 457-474.

Muchez Ph. & Corbella M.., 2012. Factors controlling the precipitation of copper and cobalt minerals in sediment-hosted ore deposits: Advances and restrictions. Journal of Geochemical Exploration,118, 38-46.

Ngoyi K., Liégeois J-P., Demaiffe D. & Dumont P., 1991. Age tardiubendien (Protérozoïque inférieur) des dômes granitiques de l'arc cuprifère zaïro-zambien. Compte Rendu de l'Académie des Sciences Paris, 313, 83-89.

Porada, H. & Berhorst, V., 2000. Towards a new understanding of the Neoproterozoic-early Palæozoic Lufilian and northern Zambezi belts in Zambia and the Democratic Republic of Congo. Journal of African Earth Sciences, 30, 727-771.

Rainaud, C., Master, S., Armstrong, R. & Robb, L., 2005. Geochronology and nature of the Palaeoproterozoic basement in the Central African Copperbelt (Zambia and the Democratic Republic of Congo), with regional implications. Journal of African Earth Sciences, 42,1-31.

Roberts, S., Palmer, M. R., Cooper, M. J., Buchaus, P. & Sargent, D., 2009. REE and Sr isotope characteristics of carbonate within the Cu-Co mineralized sedimentary sequence of the Nchanga Mine, Zambian Copperbelt. Mineralium Deposita, 44, 881-891.

Rudnick, R.L. & Gao, S., 2003. The Composition of the Continental Crust. In Holland, H.D. & Turekian, K.K. (eds.), Treatise on geochemistry, Elsevier-Pergamon, Oxford,1-64.

Selley, D., Broughton, D., Scott, R., Hitzman, M., Bull, S., Large, R., McGoldrick, P., Croaker, M., Pollington, N. & Barra, F., 2005. A New Look at the Geology of the Zambian Copperbelt. Society of Economic Geologists, 100th Anniversary Volume, 965-1000.

Torremans, K., 2011. Study of Cu-Co ore distribution and remobilization processes at the Konkola ore deposit, Zambia. Unpublished master thesis, KU Leuven, 212.

Wagner, T., Boyce, A.J. & Erzinger, J., 2010. Fluid-rock interaction during formation of metamorphic quartz veins: A REE and stable isotope study from the Rhenish Massif, Germany. American Journal of Science, 310, 645-682.

Zhong, S. & Mucci, A., 1995. Partitioning of rare earth elements (REEs) between calcite and seawater solutions at 25°C and 1 atm, and high dissolved REE concentrations. Geochimica et Cosmochimica Acta, 59, 443-453.

Manuscript received 08.11.2012, accepted in revised form 03.01.2013, available online 03.01.2013.